

# Viscous coupling effect on hydraulic conductance in a square capillary tube

Wenbo Gong<sup>a</sup>, Yang Liu<sup>a</sup>, Wenhai Lei<sup>a,b</sup>, Yang Ju<sup>c</sup>, Moran Wang<sup>a,\*</sup>

<sup>a</sup> Department of Engineering Mechanics, Tsinghua University, Beijing 100084, China

<sup>b</sup> Department of Mechanics, Royal Institute of Technology (KTH), Stockholm 100 44, Sweden

<sup>c</sup> State Key Laboratory of Coal Resources & Safe Mining, China University of Mining & Technology, D11 Xueyuan RD., Beijing 100083, China

## ARTICLE INFO

### Keywords:

Immiscible fluid flow  
Hydraulic conductance  
Viscous coupling effect  
Wetting film  
Contact angle  
Viscosity ratio

## ABSTRACT

Viscous coupling effect on pore-scale flow capacity and its impact on macroscopic flow properties in porous media remain subjects of ongoing debate. This study employs the Stokes equation in conjunction with the zero-velocity interface and continuity interface to investigate viscous coupling effect during two-phase flow through a square capillary tube. Our findings substantiate the significance of the viscous coupling effect in angular pore multiphase flows. Enhanced fluid conductance is linked to fluid viscosity ratios, contact angles, and wetting-film lengths at the pore scale. Proposing a novel upscaling approach, we formulate hydraulic conductance in a square capillary tube for multiphase flows by incorporating a viscous coupling term, and its validation is accomplished through comparison with results from lattice Boltzmann method simulations. Our scaling model predicts hydraulic conductance with a mean relative error of less than 1%, outperforming prior viscous coupling models with errors reaching up to 19%. The derived scaling model, incorporating the viscous coupling effect, holds potential for integration within pore-network models, offering an efficient and precise simulation method for characterizing two-phase flow through porous media at a representative scale.

## 1. Introduction

Multiphase flow in porous media is a fundamental phenomenon with broad implications across natural and industrial contexts, including enhanced hydrocarbon recovery, carbon dioxide storage, remediation of contaminated soils, and fuel cell technology (Atyabi and Afshari, 2019; Guo et al., 2022; Baroutaji et al., 2019; Lei et al., 2023; Liu and Wang, 2020). Due to the intricate interplay of multiphase fluids and interface dynamics, understanding fluid behavior in porous media goes beyond the conventional Darcy equation. The complexity of flow mechanisms within porous structures poses challenges in accurately describing these processes (Spurin et al., 2021; Rose, 1997; Christou et al., 2019). Scholars have explored the applicability of Darcy's law in multiphase flow and revealed that adjacent immiscible fluid flows impose mutual viscous resistance, fundamentally altering the dynamics of subsequent multiphase fluid movement. This is the predicted consequence of fluid viscous force and the no-slip boundary condition, which allows the momentum transfer across the fluid-fluid interfaces—an effect known as viscous coupling (Legait, 1983; Singhal and Somerton, 1970; Bourbiaux and Kalaydjian, 1990; Kalaydjian, 1990; Andersen et al., 2020).

The discourse surrounding the existence and influence of viscous

coupling on multiphase flow behavior in porous media has fueled ongoing debates. Experimental observations by Zarcone and Lenormand underscored the slight magnitude of enhanced fluid flow capacity due to the viscous coupling effect, being merely 0.01 in comparison to uncoupled cases (Zarcone and Lenormand, 1994). However, experiments also indicated intriguing phenomena, such as counter-current flow yielding lower effective conductance compared to co-current flow under steady-state conditions, suggesting that viscous coupling can either promote or hinder multiphase flows (Bourbiaux and Kalaydjian, 1990; Andersen et al., 2019; Ramakrishnan and Goode, 2015). In theoretical studies, Yuster illuminated the role of multiphase interface interaction in yielding relative permeability values exceeding 1, while highlighting the momentum exchange across the two-phase interface as a crucial determinant (Yuster, 1951). Numerical simulations of immiscible fluid flow in porous media unveiled non-linear behavior, particularly under high capillary numbers, where viscous coupling emerged as a significant contributing factor (Ehrlich, 1993; Gunstensen and Rothman, 1993; Solazzi et al., 2023; Qiao et al., 2018). Pore-scale analyses illuminated the substantial impact of viscous coupling on interface dynamics, including surface shear flow and ganglia remobilization, further emphasizing its pivotal role (Legait, 1983; Roman et al., 2020). The

\* Corresponding author.

E-mail address: [mrwang@tsinghua.edu.cn](mailto:mrwang@tsinghua.edu.cn) (M. Wang).

<https://doi.org/10.1016/j.advwatres.2023.104568>

Received 9 August 2023; Received in revised form 12 October 2023; Accepted 31 October 2023

Available online 3 November 2023

0309-1708/© 2023 Elsevier Ltd. All rights reserved.

failure to account for viscous coupling in immiscible fluids' permeability calculations was found to introduce discrepancies of around 30%–40% in porous media (Kalaydjian, 1990; Bentsen, 1998a,b).

Although pore-scale studies demonstrate the considerable effect of viscous coupling at the two-phase interface, this effect is relatively weak in natural porous media (Yazzan et al., 2013), leading to unresolved conflicts in the literature. Macroscopic viscous coupling effects are often represented through variations in relative permeability curves, indicative of the displacement path of immiscible fluids within porous media (Huang and Lu, 2009; Ramstad et al., 2010). The limited impact of viscous coupling in natural porous media can be attributed to the separation of two-phase fluids by solid walls, minimizing direct contact between the fluids and impeding momentum exchange across the fluid interface (Zarcone and Lenormand, 1994). Viscous coupling emerges as a result of viscous shear forces at the immiscible interface and correlates with the interface area of two-phase fluids in porous media (Rakotomalala et al., 1995; Li et al., 2005). In theoretical pore-scale analyses, a prescribed wetting film is typically introduced, enabling the coexistence of immiscible fluids within local capillaries, thereby retaining a substantial interfacial area (Shams et al., 2018). Such coexistence is particularly observed in capillaries or void structures with angular geometries, where wetting fluid flows along corners and non-wetting fluid resides in central regions, particularly under strongly wetting conditions (Primkulov et al., 2019). Transport through constricted spaces is influenced by pore geometry, flow state, and adjacent immiscible fluid properties such as viscosity ratio and capillary number (Lenormand et al., 1988). Experimental studies have demonstrated that under strong wetting conditions and low capillary numbers, the coexistence of wetting films in local zones occurs, significantly influencing viscous coupling in multiphase flow (Primkulov et al., 2019; Primkulov et al., 2021; Lei et al., 2022).

Despite extensive investigation, the origin and magnitude of viscous coupling effects in multiphase flow through porous media remain inadequately understood. The challenge lies in determining the most suitable research approach, whether experimental, numerical, or theoretical (Rose, 1997). Experimental endeavors must balance high-resolution requirements for local interfacial dynamics with the need for large-scale views to assess statistical characteristics (Lei et al., 2022). Numerical simulations are necessary to capture the complex dynamics of fluids with non-uniform viscosity ratios within angular capillaries, but they demand significant computational resources, particularly under non-uniform viscosity ratio conditions (Singhal and Somerton, 1970; Hu et al., 2017; Yiotis et al., 2007; Zhao et al., 2022; Ju et al., 2020). Direct observation of wetting flow using numerical simulations within representative element volumes (REV) in porous media remains elusive due to computational limitations (Liu and Wang, 2022a). Pore network models, serving as effective upscaling tools, predict the dynamic behavior of immiscible fluids within REV porous media (Zhao et al., 2022). However, these models struggle to accurately describe the coexistence of two phases within angular capillaries.

Initial models for immiscible fluid conductance, such as the Ransohoff-Radke scaling, introduced a dimensionless resistance factor to account for corner geometry, surface shear viscosity, and contact angle. The subsequent Patzek-Kristensen scaling model expanded this by encompassing various wettability conditions and cross-section geometries using the mathematic formula (Patzek and Kristensen, 2001), eventually applied to multiphase flow through porous media (Valvatne and Blunt, 2004). These models assume solid wall or perfect slip interfaces at the two-phase interface, well-suited for high and low viscosity ratio scenarios like water-heavy oil and water-gas systems. Nevertheless, these models neglect the impact of viscosity ratio and induced viscous coupling. Referring to the characterization of relative permeability at the macroscopic scale, the driving force acting on the total flow is divided into two independent parts, including the potential gradient within the same phase and the potential gradient within the neighboring phase, leading to a generalized matrix of the fluid

conductance (three independent coefficients) as a function of viscosity ratio and cross-section geometry (Shams et al., 2018; Dehghanpour et al., 2011). These works solidify the physical base of the fluid conductance model, but employ numerous parameters and more complex function types, leading to a relative error up to 19% between the results from the scaling model and numerical simulations. Besides, a modification factor is applied to approach the fluid conductance from the direct numerical simulations, accounting for the viscous coupling effect due to momentum transfer across the immiscible interface, based on the fluid conductance with zero-velocity interface. Theoretical efforts sought to capture the relationship between viscosity ratio and fluid conductance, yet often overlooked the effects of wettability and interface geometry (Jiang et al., 2021; Xie et al., 2017). Therefore, there's a need for a new viscous-coupling model capable of accurately predicting fluid flow states and conductance in angular capillaries.

The velocity distribution of two-phase fluids within a square tube could be solved by numerical approaches including lattice Boltzmann method, direct numerical simulation (level-set, volume of fluid, phase field) (Liu and Wang, 2022b; Rabbani et al., 2017; Sethian and Smereka, 2003). These methods offer significant advantages when applied in tracking dynamic changes in two-phase interface, accompanied with considerable computational resources. The primary objective of our research is to determine the steady-state velocity distribution under a constant pressure gradient. By utilizing finite difference method (FDM) to solve the Stokes flow with the two-phase interface equation, we can circumvent the dynamic evolution of the two-phase interface, thus directly acquiring the velocity distribution of the two-phase fluids at steady state. In this paper, we perform a series of FDM simulations and analyze fluid velocity distributions within square capillaries under diverse fluid configurations, contact angles, and viscosity ratios. Specifically, two interfacial conditions between multiphase fluids are investigated, including the zero-velocity interface and the continuity interface. Comparing FDM results for two-phase conductance under zero-velocity interface condition with previous scaling models, we evaluate the accuracy of previous models and propose an improved model for nonwetting-fluid conductance under zero-velocity interface condition, providing high accuracy as a function of fluid saturation. A dimensionless parameter, the ratio of continuity-interface conductance to that with zero-velocity interface, is defined to explore how viscous coupling effect changes over fluid configurations, contact angles, and viscosity ratios. This analysis allows us to derive new scaling models for two-phase conductance with viscous coupling. Furthermore, we validate FDM results concerning viscous coupling effects through comparison with lattice Boltzmann method simulations, introducing precise and straightforward correlations for hydraulic conductance with viscous coupling effect in immiscible fluid flows through angular capillary tubes. These correlations exhibit excellent agreement with numerical simulation results.

## 2. Method and validations

### 2.1. The equations of viscous-coupling flow

To enhance the accuracy in predicting the hydraulic conductance of immiscible fluids, we solved the velocity field of immiscible fluids by combining the Stokes equation with immiscible interface conditions. We make the assumption that the incompressible fluid flow is slow enough to disregard inertial and time-dependent terms in the Navier-Stokes equations at steady state, leading to a simplified governing equation:

$$\nabla^2 u + \frac{\nabla p - f}{\mu} = 0 \quad (1)$$

where  $u$  and  $\nabla p$  represent fluid velocity and pressure gradient, respectively, and  $f$  signifies the body force. When non-wetting fluid occupies the angular capillaries, filaments form along the corners, establishing

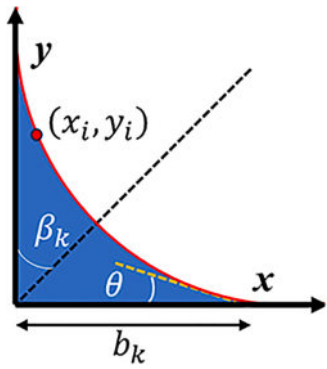


Fig. 1. The diagram of arc-meniscus flow of two-phase fluids with contact angle  $\theta$  in an angular cross-section with half angle  $\beta_k$ , where the wetting fluid occupies the corner part (blue) with the wetting-film length  $b_k$ .

translationally symmetric arc-meniscus (AMs) that delineate wetting and non-wetting fluids, as shown in Fig. 1. A governing equation is formulated for each fluid:

$$\nabla^2 u_\alpha + \frac{f}{\mu_\alpha} = 0, \quad (\alpha = w, n) \quad (2)$$

To facilitate the description,  $f$  is used to characterize the driving force  $\nabla p - f$  in the following part. For the Stokes flow in a horizontal tube, only horizontal component of two-phase velocity in the  $z$ -axis is non-zero and varies in the  $x$ - $y$  plane owing to the no-slip boundary condition in the solid wall. At steady state, the velocity distribution and the

two-phase interface for arc-meniscus flow remain unchanged in the tube, and the interface morphology is determined by the cross-section geometry (half angle  $\beta_k$ ), contact angle  $\theta$ , and wetting-film length  $b_k$ , as shown in Fig. 1. The spatial distribution of two-phase interface could be described as:

$$\left(x_i - \frac{b_k \cos \theta \cos \beta_k}{\cos(\theta + \beta_k)}\right)^2 + \left(y_i - \frac{b_k \cos \theta \sin \beta_k}{\cos(\theta + \beta_k)}\right)^2 = \left(\frac{b_k \sin \beta_k}{\cos(\theta + \beta_k)}\right)^2 \quad (3)$$

where  $(x_i, y_i)$  represents the interface location in the corner  $k$ .

Patzek and Kristensen's work (Patzek and Kristensen, 2001) introduced three distinct boundary conditions along the AM:

- (1) the no-slip condition (or zero-velocity condition) implies infinite surface shear viscosity at the interface, resulting in zero interfacial velocity:

$$u_\alpha = 0 \quad (4)$$

- (2) the perfect-slip condition characterizes liquid-gas interfaces, where no momentum transfer occurs across the AM:

$$\nabla u_\alpha \cdot \vec{n}_\alpha = 0 \quad (5)$$

- (3) the continuity condition does not impose constraints on the viscosity of immiscible fluids, ensuring continuity in velocity and shear stress:

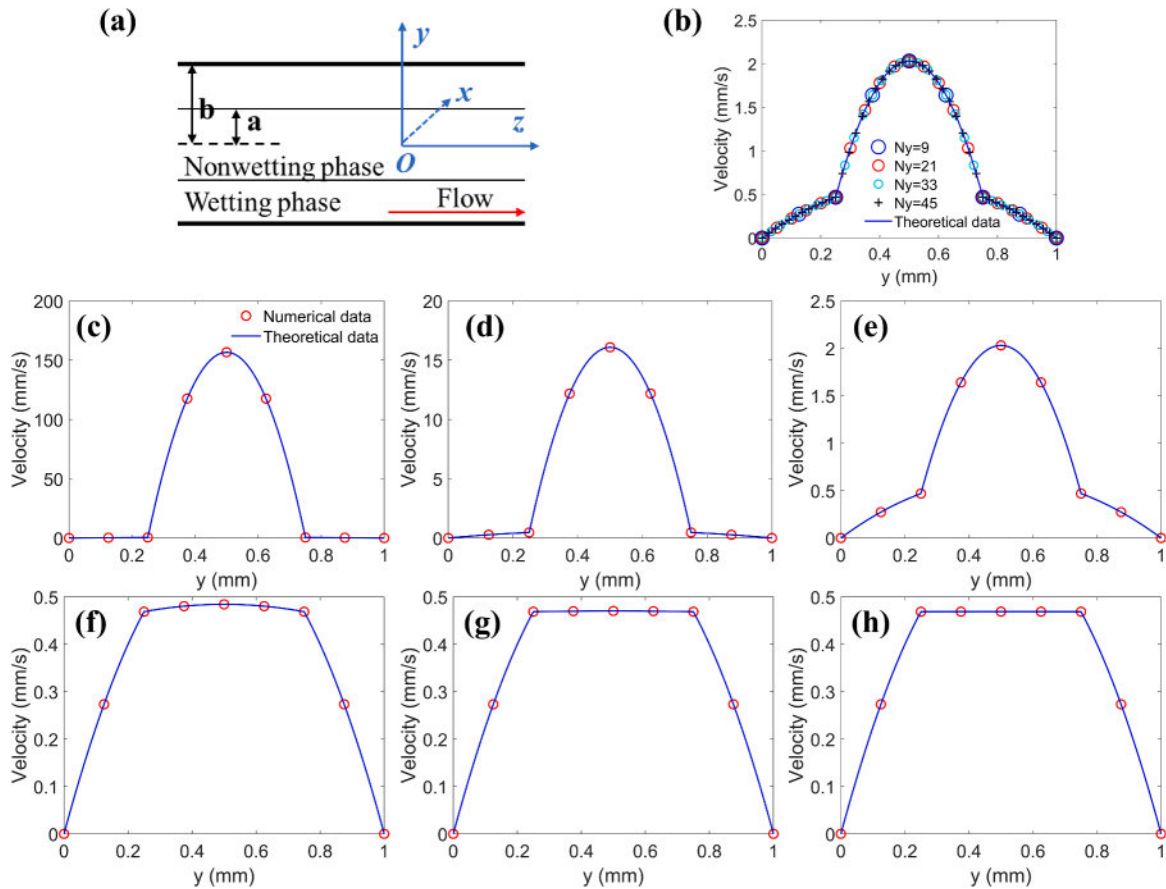


Fig. 2. Validation of velocity profile for the two-phase co-current flow. (a) schematic diagram of two-phase co-current flow; (b) validation of grid-independence for two-phase co-current flow; subfigures (c)-(h) are the velocity profile of two-phase fluids with viscosity ratio 0.001, 0.01, 0.1, 10, 100, and 1000, respectively, where nine nodes are used to mesh the computation domain ( $N_y=9$ ). The numerical and theoretical results are labeled as red circles and blue lines.

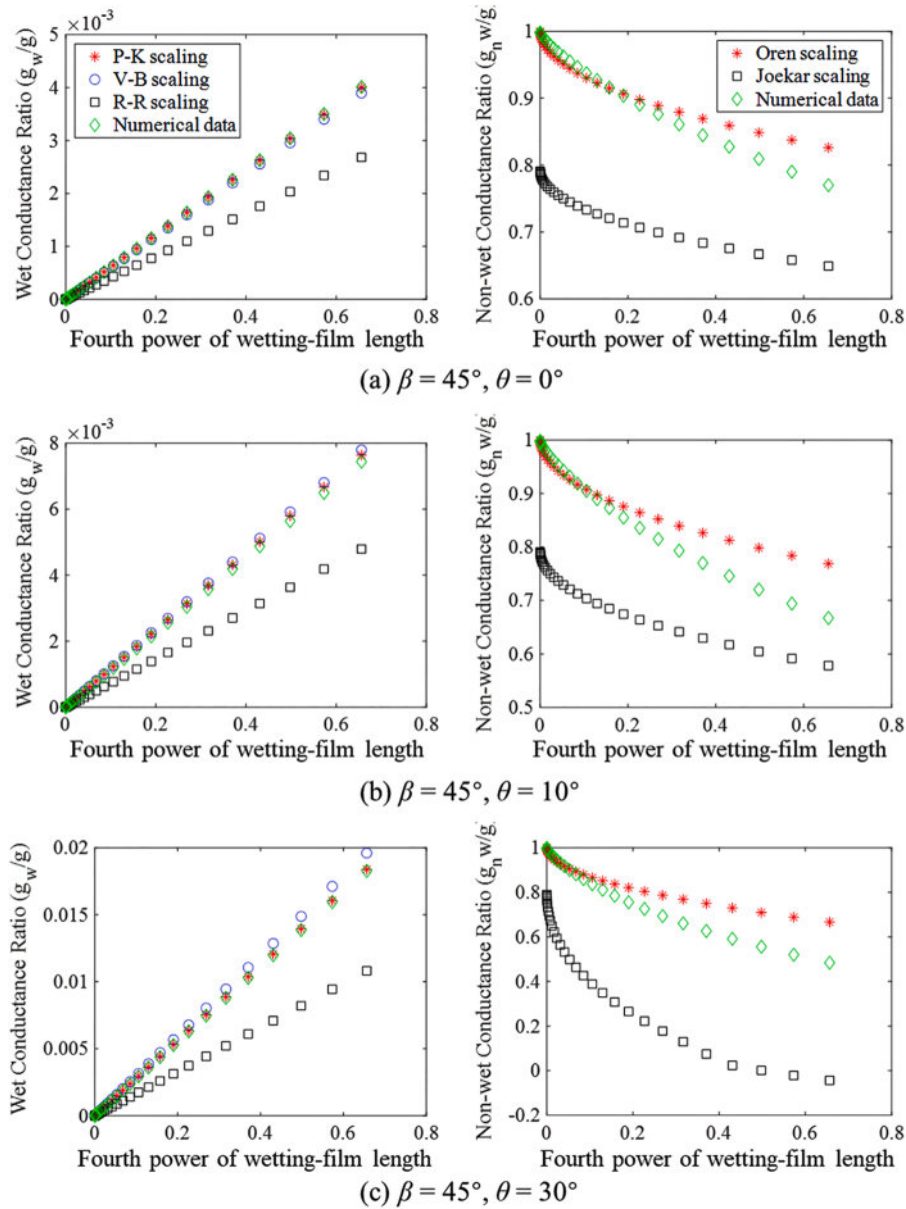


Fig. 3. Comparison of hydraulic conductance of two-phase fluids in a square cross-section. The left and right columns are the wetting and non-wetting fluid conductance, respectively. Cases (a)-(c) represent the fluid conductance with contact angles  $0^\circ$ ,  $10^\circ$ , and  $30^\circ$ .

$$\mu_w \nabla u_w \cdot \vec{n}_w = \mu_n \nabla u_n \cdot \vec{n}_n \quad (6)$$

This study investigates the viscous-coupling effect of immiscible fluids using the continuity condition. Both the wetting and non-wetting fluids adhere to the same partial differential equation scheme, necessitating continuous velocity at the immiscible interface. Consequently, the governing equation transforms into a simplified form:

$$\nabla^2 u + f^* = 0 \quad (7)$$

where  $f^* = f/\mu_\alpha$  for the computational nodes occupied by the  $\alpha$ -phase fluid.

Given the symmetric nature of fluid flow within a square capillary tube, our simulations focus on a quarter of the square tube. As such, a symmetric boundary condition is applied to fluid nodes, while a no-slip boundary condition is imposed on solid nodes. To validate the accuracy

of these boundary conditions, we compared single-phase conductance within a square tube between numerical data and scaling results derived from published empirical models (Fig. B1 in Appendix B).

## 2.2. Validation of continuity interfacial condition

The influence of the coexisting phase on fluid flow state is characterized by the interfacial boundary condition, which finds illustration in the context of two-phase co-current flow within a straight channel formed by infinite parallel plates, as depicted in Fig. 2(a). The configuration involves a non-wetting fluid with viscosity  $\mu_n$  occupying the central region, while a wetting fluid with viscosity  $\mu_w$  resides on both sides adjacent to the plates. Both fluids are propelled by an identical pressure gradient  $\nabla p$ . Xie et al. (2017) provided the theoretical solution for the velocity distribution of the two fluids:

$$\text{For } 0 < y < a, u_{nw} = \frac{\nabla p}{2\mu_w} (b^2 - a^2) + \frac{\nabla p}{2\mu_{nw}} (a^2 - y^2)$$

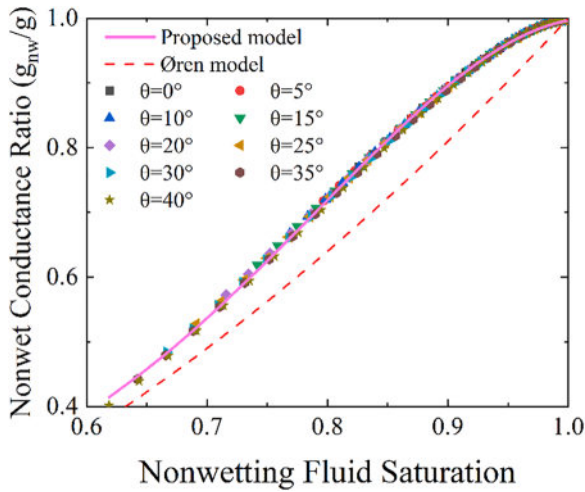


Fig. 4. Comparison of nonwetting-fluid conductance ratio calculated from the proposed scaling model and the numerical results with different contact angles from 0° to 40°. The pink line and red dash line stand for the proposed scaling model and Øren scaling model.

$$\text{For } a < y < b, u_w = \frac{\nabla p}{2\mu_w} (b^2 - y^2)$$

where  $b$  is the half distance between two infinite parallel plates, and  $a$  is the half width of central region occupied by nonwetting fluid.

Discretization of the continuity condition at the immiscible interface is accomplished using the second-order upwind scheme. The discretization direction of the fluid viscous term depends on the normal orientation of the immiscible interface, represented by the unit vector  $(n_x, n_y)$ . The continuity condition is reconstructed as

$$\left( \hat{\mu} \frac{\partial u_{mw}}{\partial x} - \frac{\partial u_w}{\partial x} \right) * n_x + \left( \hat{\mu} \frac{\partial u_{mw}}{\partial y} - \frac{\partial u_w}{\partial y} \right) * n_y = 0 \quad (8)$$

where viscosity ratio is denoted as  $\hat{\mu} = \mu_n/\mu_w$ . When the normal vector component  $n_x > 0$ :

$$\begin{aligned} \frac{\partial u_{mw}}{\partial x} &= \frac{-u_{i+2,j} + 4u_{i+1,j} - 3u_{i,j}}{2dx} \\ \frac{\partial u_w}{\partial x} &= \frac{3u_{i,j} - 4u_{i-1,j} + u_{i-2,j}}{2dx} \end{aligned} \quad (9)$$

Conversely, when the normal vector component  $n_x < 0$ :

$$\begin{aligned} \frac{\partial u_{mw}}{\partial x} &= \frac{3u_{i,j} - 4u_{i-1,j} + u_{i-2,j}}{2dx} \\ \frac{\partial u_w}{\partial x} &= \frac{-u_{i+2,j} + 4u_{i+1,j} - 3u_{i,j}}{2dx} \end{aligned} \quad (10)$$

The same discretization scheme is used for the y-axis partial term. Combing the governing equation Eq. (7) and interfacial condition equation (Eqs. (9) and (10)), the velocity field is computed using FDM. The discrete scheme of the governing equation is referred to Eq. (B.1) in Appendix B. Extending the investigation across viscosity ratios ranging from 0.001 to 1000, a comparison of perpendicular velocity profile indicates that the FDM results math well with the theoretical solution, as presented in Fig. 2.

### 3. Results and discussion

#### 3.1. The zero-velocity interfacial condition

The zero-velocity boundary condition delineates a distinctive fluid interface existing between wetting and non-wetting phases. In this configuration, a fluid endowed with infinite viscosity can be analogized

as a zero-velocity wall when compared to another immiscible fluid characterized by a relatively lower viscosity. While preceding investigations have offered prognostications regarding hydraulic conductance in the corner flow of wetting fluids (wetting film), accurate predictions concerning hydraulic conductance of non-wetting fluids have been scant. To address this, consolidated scaling models pertaining to fluid conductance within an angular tube are introduced for both single-phase and two-phase fluids in Appendix A. In this section, the fluid velocity field is solved through the integration of governing fluid flow equations (Eq. (7)) and the zero-velocity interfacial condition (Eq. (4)). A dimensionless parameter, the wetting film length, is employed, which signifies the ratio of the meniscus-apex distance to the inscribed circle radius in a square capillary. Its values span from 0.03 to 0.9, with contact angles set at 0°, 10°, and 30°. The viscosity ratio for all simulations remains fixed at 10 ( $\mu_n/\mu_w = 10$ ). The corresponding conductance of two-phase fluids is computed as:

$$g_\alpha = \frac{Q_\alpha}{f} = \frac{\int u_\alpha dA_\alpha}{f} = \frac{1}{f} \sum u_\alpha * dx dy \quad (11)$$

where  $Q_\alpha$  is flux of fluid  $\alpha$  in the cross-section, and the  $u_\alpha$ ,  $A_\alpha$  are fluid velocity and element area of the fluid  $\alpha$  nodes in the FDM simulations.

The hydraulic conductance of the wetting fluid is juxtaposed against previous predictions, including the (Patzek and Kristensen, 2001), the Valvatne-Blunt scaling (Valvatne and Blunt, 2004), and the Ransohoff-Radke scaling (Ransohoff and Radke, 1988), as shown in Fig. 3. The horizontal ordinate “Fourth power of wetting-film length” means  $b_k^4$ , and the vertical ordinate “Conductance Ratio” stands for the ratio of each fluid conductance to the single-phase conductance ( $g_w/g$ ), where the single-phase conductance is calculated as Eq. (A.3). The discrepancy of fluid conductance between previous scaling models and numerical results are observed under various wetting-film lengths and contact angles. As depicted in Fig. 3, our numerical findings concerning wetting-fluid conductance using the FDM approach closely align with prior empirical models across varying contact angles and multiphase distributions, with the exception of the Ransohoff-Radke scaling. With increasing contact angles, deviations emerge between the hydraulic conductance predicted by the Valvatne-Blunt scaling and our numerical data, while congruence is observed with the Patzek-Kristensen scaling. Furthermore, a comparison between computed non-wetting-fluid conductance results and the empirical models proposed by (Øren et al., 1998) and (Joekar-Niasar et al., 2010) highlights substantial discrepancies. This underscores the need for a novel scaling model that precisely anticipates non-wetting fluid hydraulic conductance within a square tube.

The zero-velocity interface condition nullifies the viscous coupling effect by employing a solid wall, rendering the fluid hydraulic conductance unaltered by the viscosity ratio. Our primary focus resides in assessing the impact of contact angle and wetting-film length on fluid conductance for the corner flow with geometrical constraint  $\theta + \beta_k < \pi/2$ . The saturation of non-wetting fluid  $S_n$ , positioned within the bulk region of the square cross-section, can be formulated as a function of contact angle  $\theta$  and wetting-film length  $b_k$  in the cross-section corner  $k$  with half angle  $\beta_k$  (Qin and van Brummelen, 2019):

$$S_n = 1 - \sum_{k=1}^n \left( \frac{b_k^2 \sin \beta_k}{\cos(\theta + \beta_k)} \right)^2 \left[ \frac{\cos(\theta + \beta_k) \cos \theta}{\sin \beta_k} + \theta + \beta_k - \frac{\pi}{2} \right] \quad (12)$$

Analysis reveals a consistent trend in the hydraulic conductance of non-wetting fluid as fluid saturation increases under diverse contact angles, as depicted in Fig. 4. The red dashed line denotes the prediction of nonwetting-fluid conductance using the Øren scaling approach, demonstrating weaker alignment with numerical data in comparison to the pink line, which represents the proposed scaling model (Eq. (13)). As non-wetting fluid infiltration progresses, the conductance reaches a theoretical maximum boundary, as predicted by (Patzek and Kristensen, 2001). To ensure a dimensionless value ranging from 0 to 1, a sinusoidal

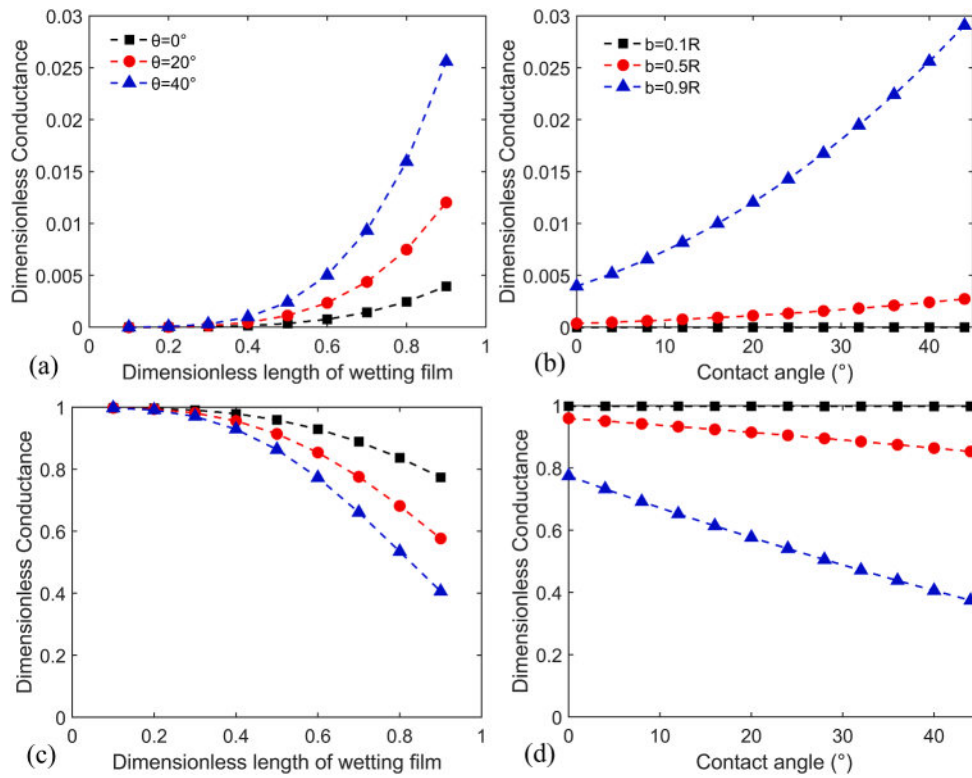


Fig. 5. The impact of contact angle and film length in the hydraulic conductance with zero-velocity interface: (a)-(b) for wetting fluid, (c)-(d) for non-wetting fluid.

function is employed. Scaling coefficients are deduced by fitting saturation and dimensionless hydraulic conductance of non-wetting fluid, yielding the new scaling model:

$$g_{n0} = 0.5623GA^2 \sin(3.6S_n^2 - 3S_n + 0.9) / \mu_n \quad (13)$$

The mean relative error between the results from the scaling model and numerical data is 0.33%, attesting to the accuracy of our model in capturing non-wetting fluid conductance across various flow configurations. This foundation serves as a springboard for subsequent investigations into non-wetting phase conductance coupled with the viscous coupling effect.

Despite the absence of momentum transfer across the immiscible interface within the context of a zero-velocity interface, the hydraulic conductance of immiscible fluids still experiences influence from both the contact angle and wetting film length, resulting from the fluid configuration variation, as delineated in Eq. (12). Regarding the wetting fluid, hydraulic conductance exhibits a positive correlation with both wetting film length and contact angle, while a negative relationship for the non-wetting fluid, as illustrated in Fig. 5. In comparison with fluid distribution at lower contact angle, a more pronounced increase or decrease in hydraulic conductance ensues with the elevation of wetting film length, particularly under higher contact angles, impacting the wetting and non-wetting fluids, respectively. The hydraulic conductance of both wetting and non-wetting fluids remains relatively constant for minute wetting films but experiences significant changes for longer wetting films when varying contact angles in the context of immiscible fluids coexisting within an angular capillary.

### 3.2. The continuity interfacial condition

#### 3.2.1. The effect of interfacial condition

To examine the influence of interfacial condition in the two-phase conductance, we delve into the immiscible flow within a square capillary using the FDM, enforcing continuity of velocity and shear stress across the immiscible interface. In the modeling, the wetting-fluid

viscosity remains constant, while the viscosity of the non-wetting fluid is varied to probe the effect of viscosity ratio on immiscible fluid flow in a square capillary. Particularly, the fluid contact angle is set at 0°, and the wetting-film length spans 0.9 times the inscribed radius of the square capillary. Within this context, the interfacial conditions exert a discernible influence on the immiscible fluid flow, resulting in diverse features in the quarter-section of the square cross-section under different viscosity ratios, as depicted in Fig. 6. The white and dark curves delineate the immiscible interfaces corresponding to zero-velocity and continuity conditions, respectively. A conspicuous observation is the recurring non-monotonic variation of the velocity profile along the diagonal axis of the square capillary within the wetting-phase zone governed by the zero-velocity interface. Conversely, this non-monotonic trend within the wetting-phase zone under continuity interface is evident only for fluid conditions featuring the highest viscosity ratio ( $M = 1000$ ). In that case, a slight influence on wetting-fluid velocity due to interfacial conditions becomes apparent, coupled with an enhancement in non-wetting-fluid velocity. Under the lowest viscosity ratio ( $M = 0.001$ ), velocity profiles between different interfacial conditions have comparable magnitudes and almost entirely overlap along the normal axis. Notably, within the subfigure, it is evident that the velocity of wetting fluid featuring the continuity interface surpasses that characterized by the zero-velocity interface. This phenomenon can be attributed to the fixed driving force exerted on the immiscible fluids along the same direction, resulting in a heightened fluid velocity within the square capillary, driven by the drag force of high-velocity fluid acting upon low-velocity fluid, which resonates with prior research on co-current imbibition (Bourbiaux and Kalaydjian, 1990).

#### 3.2.2. The effect of fluid configuration

(Ransohoff and Radke, 1988) elucidated that alterations in fluid distribution and contact angle will change the two-phase fluid flow state on the cross-section, and the surface shear viscosity also will affect the boundary conditions (immiscible interface) imposed by the two-phase interface on different fluids. Hence, a comprehensive analysis of their

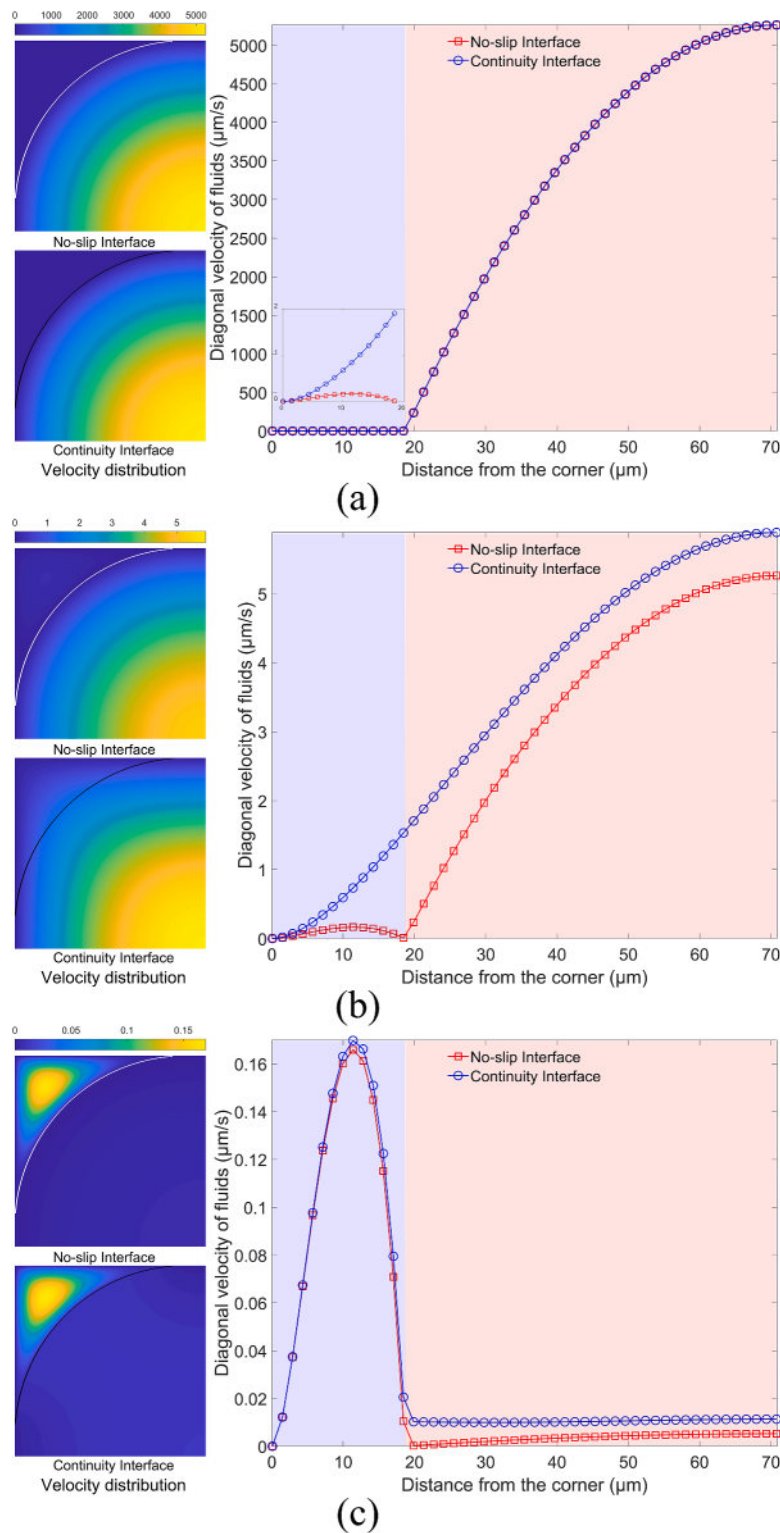


**Fig. 6.** The comparison of fluids velocity distribution with zero-velocity interface condition and continuity interface condition in a quarter of square cross-section with different viscosity ratios: (a)  $M = 0.001$ ; (b)  $M = 1$ ; (c)  $M = 1000$ . The contact angle and wetting-film length in the three cases are  $0^\circ$  and  $0.9$ .

impact on the viscous coupling effect is imperative. It is evident that the zero-velocity boundary condition curtails momentum transfer across the immiscible interface, and the influence of wetting-film length and contact angle is manifested through changes in fluid saturation. Conversely, when the continuity interfacial condition is considered, the onset of the viscous coupling effect within immiscible flow through a square capillary becomes evident. The enhancement of fluid flow capacity due to the

viscous coupling effect is relevant to the wetting-film length and contact angle. To reveal this intrinsic relationship, we introduce the dimensionless conductance of immiscible fluids, denoted as  $\hat{g}_\alpha$  ( $\alpha = w, n$ ), to quantify the viscous coupling effect on fluid conductance, which is the ratio of hydraulic conductance with continuity interface  $g_\alpha$  to that with zero-velocity interface  $g_{\alpha 0}$ , i.e.,  $\hat{g}_\alpha = g_\alpha / g_{\alpha 0}$ .

In subSection 3.1, we previously established that the hydraulic

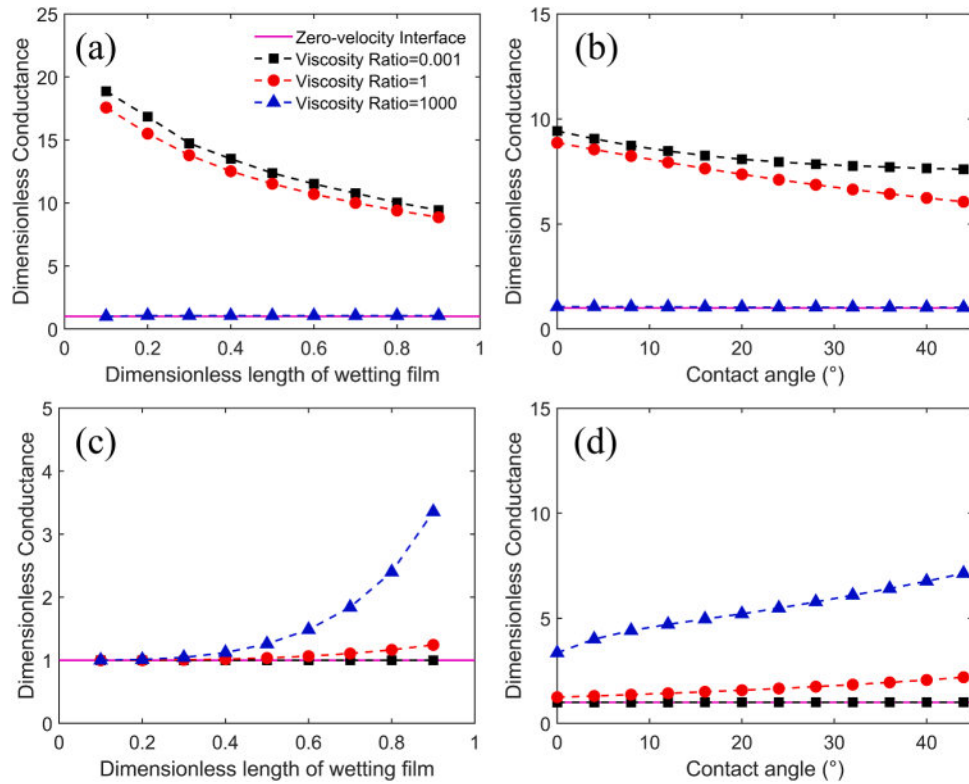


Fig. 7. The Enhanced hydraulic conductance of fluids in a square cross-section: (a)-(b) for wetting fluid, (c)-(d) for nonwetting fluid. The contact angle is set as zero in (a) and (c), and the wetting-film length equals 0.9 in (b) and (d).

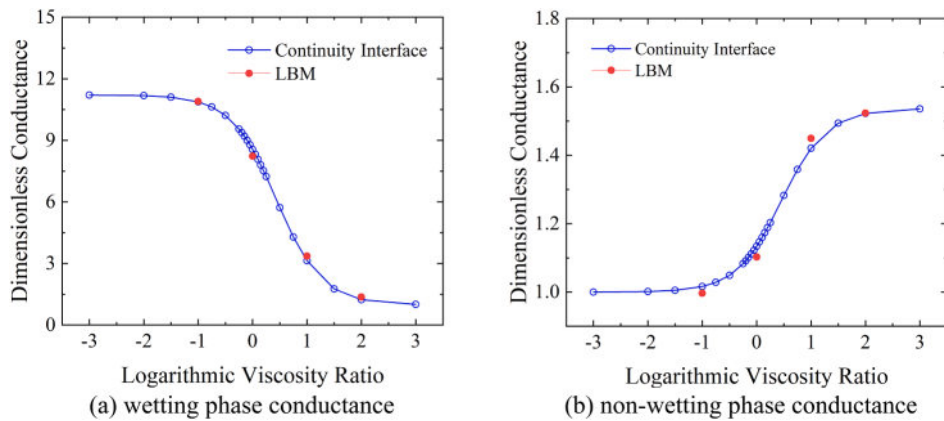


Fig. 8. Effect of viscosity ratio on the enhancement of two-phase conductance. ( $\theta = 30^\circ$ ,  $b = 0.5$ ).

conductance at a zero-velocity interface exhibits a positive relationship with both wetting film length and contact angle for the wetting fluid, while conversely, it shows a negative correlation with the nonwetting fluid. Building upon these findings, our analysis of the continuity interfacial condition yields further insights. We observe that the increase in hydraulic conductance resulting from the influence of viscous coupling is negatively associated with the expanding wetting-film length and contact angle for the wetting fluid in Fig. 7. This observation suggests that the rise in wetting-fluid conductance is primarily attributable to the increased fluid saturation and viscous coupling effects. Furthermore, it is worth noting that the impact of viscous coupling on conductance enhancement diminishes as the wetting-film length and contact angle increase. Moreover, the increasing viscosity ratio weakens the hydraulic conductance enhancement induced by the wetting-film length and contact angle for the wetting fluid but strengthens their

impact in the non-wetting-fluid conductance. In particular, the discrepancy of hydraulic conductance between the zero-velocity and continuity interfacial conditions disappears when the viscosity ratio reaches an ultimate value. For instance, when the viscosity ratio equals or exceeds 1000 ( $M \geq 1000$ ), the hydraulic conductance of wetting fluid exhibits minimal alteration during the immiscible flow with the continuity interface, in which the non-wetting fluid with tremendous viscosity could be regarded as a solid wall due to the extremely slow velocity. Similarly, under  $M = 0.001$ , the steady flow of the wetting fluid, characterized by substantial viscosity, can be approximated as a solid wall compared to the high-velocity flow of the non-wetting fluid under the influence of continuity shear forces at the immiscible interface. These findings validate the simplifications applied to the flow dynamics of immiscible fluids coexisting within an angular capillary under conditions where fluid viscosity ratios reach extreme values, as

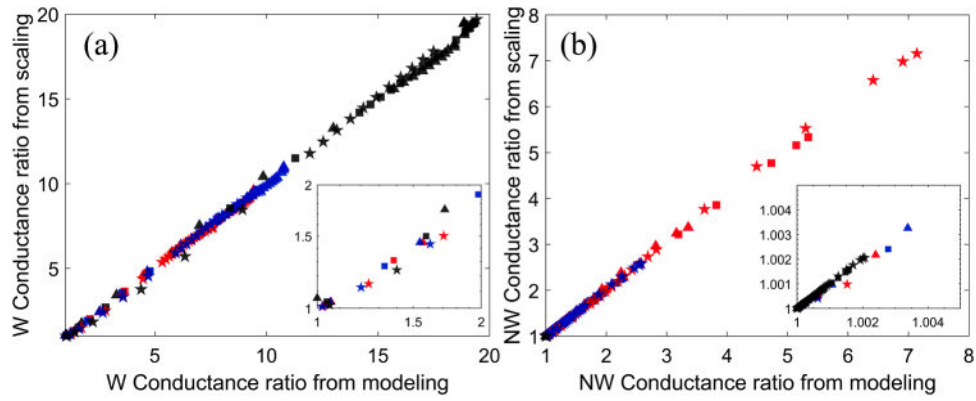


Fig. 9. The fitting results of fluid conductance in a square cross-section using the logistic-type function: (a) wetting fluid, (b) non-wetting fluid, where the coefficients in the function are discrete points. The symbols of triangular, square, and pentagram stand for contact angles of  $0^\circ$ ,  $20^\circ$ , and  $40^\circ$ ; the colors black, blue, and red represent wetting-film lengths  $b = 0.1, 0.5, \text{ and } 0.9$ .

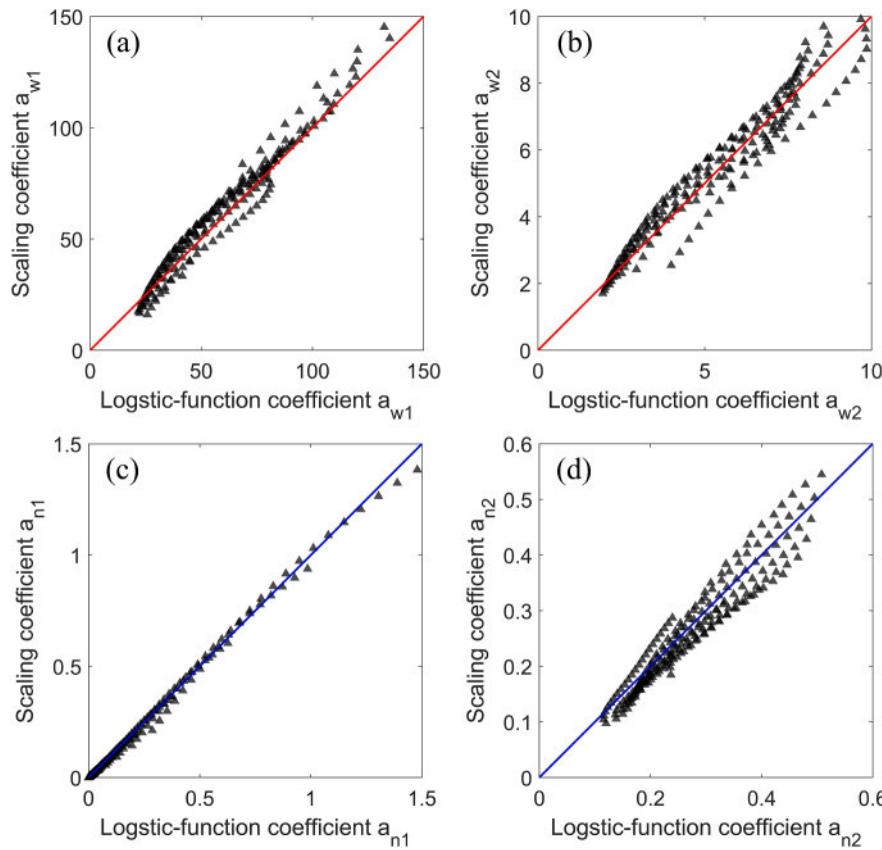


Fig. 10. The scaling of the coefficients in the logistic-type function using a mathematic formulation for the wetting fluid: (a) coefficient  $a_{w1}$ , (b) coefficient  $a_{w2}$ , and non-wetting fluid: (c) coefficient  $a_{n1}$ , (d) coefficient  $a_{n2}$ .

observed in systems such as liquid-gas and water-heavy oil (Patzek and Kristensen, 2001; Valvatne and Blunt, 2004).

### 3.2.3. The effect of viscous coupling

It is observed that the viscosity ratio affects the enhancement of hydraulic conductance of immiscible fluids due to the momentum transfer across the immiscible interface. To investigate this effect comprehensively, we conducted simulations of immiscible fluid flow under different viscosity ratios ( $M = 0.1, 1, 10, 100$ ) using the lattice Boltzmann method (LBM) with color-gradient model capable of automatically handling the immiscible interface for the viscous coupling effect (Huang and Lu, 2009; Ramstad et al., 2010; Li et al., 2005; Xie

et al., 2017; Huang et al., 2009). The simulation setup involved the application of periodic boundary conditions at the inlet and outlet of the square capillary. The immiscible fluids coexisted within a square cross-section with a side length of 2000 lattice units. The contact angle was set at  $30^\circ$ , and the wetting film length was set to 500 lattice units. Our previous work has validated the LBM model (Ju et al., 2020), and we employed it in this study to ascertain the accuracy of two-phase conductance attributed to the viscous coupling effect. As shown in Fig. 8, a comparison of dimensionless conductance of immiscible fluids shows a good agreement between LBM data and FDM results. The semi-logarithmic plots reveal the impact of the viscous coupling effect on hydraulic conductance, manifesting as a negative correlation for the

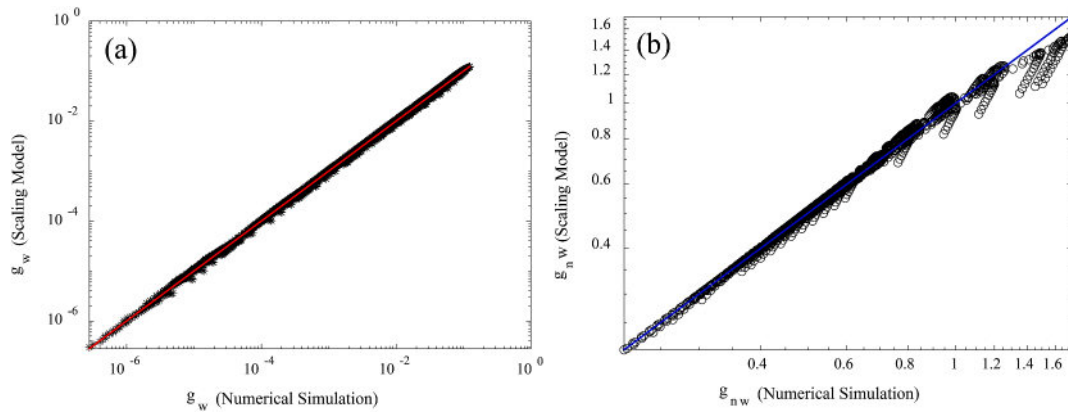


Fig. 11. Comparison of the predicted values of the scaling model with the numerical values of the fluid conductance considering the viscous coupling effect under various wettability conditions, wetting-film length, and viscosity ratios for (a) the wetting fluid, and (b) the non-wetting fluid. The symbols represent the comparison points, and the colorful lines represent the standard line  $y = x$ .

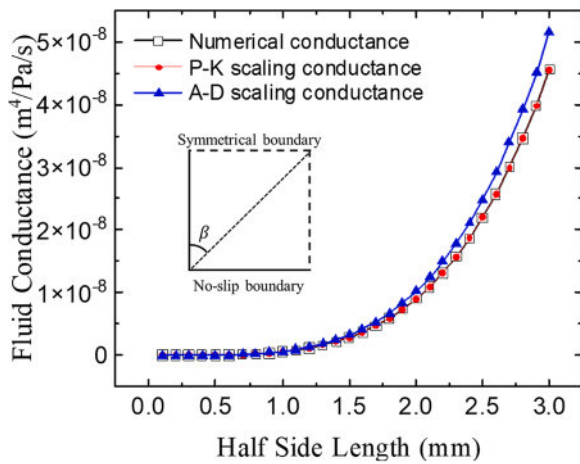


Fig. B.1. Validation of the single-phase conductance in the FDM simulations. The results from the FDM simulation, the Patzek-Kristensen scaling, and the Azzam and Dullien scaling are plotted using the black, red, and blue labels, respectively, in which a quarter of the square cross-section is computed ( $\beta = 45^\circ$ ).

wetting fluid and a positive correlation for the non-wetting fluid. It is noteworthy that the hydraulic conductance enhancement varies greatly with a viscosity ratio ranging from 0.1 to 10, eventually stabilizing at a plateau for extremely large viscosity differences. In Fig. 8, the hydraulic conductance of wetting fluid displays variations exceeding 10 times within the fluid configuration ( $\theta = 30^\circ$ ,  $b = 0.5$ ). Meanwhile, the conductance enhancement of non-wetting fluid reaches 1.5 times in Fig. 8(b), and even up to 8 times in Fig. 7(d). Besides, the viscous coupling dominates the wetting-fluid flow ( $\hat{g}_w > 1$ ) when the viscosity ratio decreases. We observe that the influence of viscous coupling is notably significant in wetting-phase flow under conditions of shorter wetting-film length, reduced contact angle, and lower viscosity ratio. Likewise, a substantial impact on nonwetting-phase conductance is evident under circumstances featuring longer wetting-film length, diminished contact angle, and lower viscosity ratio. These observations underscore the non-negligible influence of the viscous coupling effect on hydraulic conductance in immiscible fluids, which is also notably susceptible to other parameters like wetting-film length and contact angle. Our subsequent efforts will involve the formulation of a mathematical model to capture the intricate relationship between hydraulic conductance, fluid configuration, and viscosity ratio.

### 3.2.4. Scaling of hydraulic conductance

It is well understood that each phase's flow influences the other due to the viscous coupling at the two-phase interface. The total flow of each phase arises from two distinct driving forces: firstly, the potential gradient within the same phase, and secondly, the potential gradient within the neighboring phase. In this study, we employ the concept of a zero-velocity interface condition to elucidate the correlation between each phase's flow and the pressure gradient within the same phase in a square tube. Furthermore, the concept of viscous coupling is harnessed to formulate an expression that links fluid flow to the potential gradient of the adjacent phase. As a result, the conductance of each phase ( $g_\alpha$ ) is divided into two components: the fluid conductance associated with the potential gradient within the same phase ( $g_{\alpha 0}$ ) and another component linked to viscous coupling  $g_{\alpha, v} = g_{\alpha 0} \hat{g}_\alpha - g_{\alpha 0}$ . The formulation of conductance  $g_{\alpha 0}$  could be obtained by Eqs. (13) and (A.5). Previous research has suggested that the augmentation of wetting-fluid conductance due to viscous coupling reaches a maximum when dealing with two fluids featuring substantial viscosity disparities (Patzek and Kristensen, 2001; Dehghanpour et al., 2011; Xie et al., 2017). Fig. 8 further illustrates this observation. Our analysis supports the utilization of the logistic function (Eq. (14)) as a suitable means to depict the influence of viscosity ratio on two-phase conductance. Consequently, in this section, we establish logistic models to relate the dimensionless hydraulic conductance  $\hat{g}_\alpha$  to fluid viscosity ratio  $M$ , with the model parameters being considered as a function of the fluid configuration ( $\theta, b$ ):

$$\hat{g}_\alpha = \frac{a_1}{a_2 + e^{a_3 \hat{\mu}}} + a_4 \tag{14}$$

where  $\hat{g}_\alpha$  represents the dimensionless conductance of fluid  $\alpha$ ,  $\hat{\mu} = \log M$  is the logarithmic ratio of nonwetting-fluid viscosity to wetting-fluid viscosity, and  $a_1, a_2, a_3, a_4$  are the parameters relating to the wetting-film length and contact angle.

For multiphase flow involving an arc-meniscus interface, the non-wetting fluid, characterized by infinite viscosity, can be approximated as a solid wall in comparison to the flow behavior of the wetting fluid. Under such circumstances, the role of the viscous coupling effect in enhancing wetting fluid conductance is practically negligible, rendering its dimensionless value  $\hat{g}_w = a_4 = 1$ . Our FDM simulations encompass immiscible fluid flow coexisting within a square capillary, varying the contact angle from  $0^\circ$  to  $44^\circ$  in  $1^\circ$  increments, altering the dimensionless length of the wetting film  $b$  from 0.1 to 0.9 in 0.1 increments, and ranging the logarithmic viscosity ratio from  $-3$  to  $3$ . Herein, the logistic function is used to fit the variation of the hydraulic conductance at each condition with an increasing viscosity ratio. Initial fitting outcomes of the coefficients indicate that the coefficient  $a_3$  for wetting-fluid conductance ranges from 2.5 to 2.61, prompting us to standardize this

coefficient at the mean value of 2.56 for a simplified equation. The revised fitting expression for wetting fluid conductance is formulated as:

$$\hat{g}_w = \frac{a_{w1}}{a_{w2} + e^{2.56\bar{\mu}}} + 1 \quad (15)$$

For the non-wetting-fluid conductance considering the impact of the viscous coupling effect, the scaling model is given by:

$$\hat{g}_n = \frac{a_{n1}}{a_{n2} + e^{-2.44\bar{\mu}}} + 1 \quad (16)$$

To assess the precision of the logistic model and the choice of coefficient  $a_3$ , we conduct a comparison between the hydraulic conductance from the scaling formulas Eqs. (15) and (16) and the results from FDM modeling. This comparative analysis takes into account the effects of contact angle, wetting-film length, and viscosity ratio. As illustrated in Fig. 9, where black, blue, and red correspond to film lengths  $b = 0.1, 0.5$ , and  $0.9$ , respectively, and triangular, square, and pentagram symbols signify contact angles of  $0^\circ, 20^\circ$ , and  $40^\circ$ , respectively, the markers closely align with the  $y = x$  line, which demonstrates the accurate predictive capability of the scaling models for hydraulic conductance in immiscible fluids within a square capillary, even within the range approaching 1, characterized by substantial viscosity disparities between the two fluids.

Addressing the challenge of establishing the interrelation between coefficients  $a_{\alpha 1}$  and  $a_{\alpha 2}$  with respect to the wetting-film length and contact angle necessitates further investigation. As depicted in Fig. 7, the dimensionless value of the two-fluid conductance manifests an approximately linear association with the contact angle. A geometrical constant  $E_1$ , defined as  $E_1 = \cos(\theta + \beta)/\sin\beta$  ( $\beta$  is the half angle of the cross-section) in (Al-Futaisi and Patzek, 2003), demonstrates a more precise linear dependence on the dimensionless conductance of immiscible fluids. A suitable functional form that links hydraulic conductance and the wetting-film length has yet to be identified. Consequently, we have employed exponential and power functions to delineate the variation of coefficients  $a_{\alpha 1}$  and  $a_{\alpha 2}$  concerning contact angles and the wetting-film length. The comparison of these coefficients calculated from our scaling models and numerical simulation is shown in Fig. 10. The modified formulas of hydraulic conductance, accounting for the viscous coupling effect in a square capillary, are described:

$$g_w = g_{w0} * \left( \frac{(60E_1 + 14)b^{-0.33}}{(5E_1 + 1.5)e^{0.5b} + e^{2.56\bar{\mu}}} + 1 \right) \quad (17)$$

$$g_n = g_{n0} * \left( \frac{(-1.7E_1 + 2)b^{3.3}}{(-0.4E_1 + 0.6)e^{-0.8b} + e^{-2.44\bar{\mu}}} + 1 \right) \quad (18)$$

To elucidate the effect of viscous coupling on immiscible fluid flow, the correlation factor encompasses the impact of contact angle, the wetting-film length, and the viscosity ratio. Fig. 11 provides a comparative analysis between the predicted values for the viscous coupling conductance, based on the proposed scaling model, Eqs. (17) and (18), and the numerical results, for both wetting fluid and non-wetting fluids. One can observe that the scaling models exhibit commendable predictive accuracy for hydraulic conductance. The mean relative errors for hydraulic conductance stand at 0.4% and 0.8% for wetting fluid and non-wetting fluid, respectively.

## Appendix A: The empirical models of fluid conductance in a capillary tube

In the pore network model (Joekar-Niasar et al., 2010), fluid conductance  $g$  is the key parameter to estimate the volumetric flux of fluid in the transient state, which is not only related to the geometrical parameters of pore throat but also the spatial occupancy and viscosity ratio of two fluids.

Azzam and Dullien (Azzam and Dullien, 1977) provided an equivalent pore radius for fluid conductance based on the Hagen-Poiseuille equation:

## 4. Conclusions

In this study, we have undertaken an investigation into the viscous coupling effect within a square capillary, encompassing diverse fluid arrangements and viscosity ratios. By comparing velocity distribution and hydraulic conductance under various interface conditions, we have discerned the pivotal role of momentum transfer across the immiscible interface in the context of viscous coupling. The wetting-phase conductance is notably enhanced under conditions of shorter wetting-film length, reduced contact angle, and lower viscosity ratio. The significant contrast in hydraulic conductance between continuity and zero-velocity interfaces can be attributed to the conventional treatment of the zero-velocity interface as a solid boundary, which results in the exclusion of momentum transfer across the two-phase interface.

We have solved the two-phase Stokes flow in a square capillary and formulated mathematical models for hydraulic conductance, delineating scenarios both without and with the viscous coupling effect. The wetting-fluid conductance without viscous coupling effect is validated by previous mathematic models, and a novel model has been posited to capture the non-wetting-fluid conductance with heightened precision. Through the application of the continuity condition at the immiscible interface, we take into account the viscous coupling effect in the scaling model of hydraulic conductance of immiscible fluids, which are validated by numerical results for a wide range of fluid configurations and viscosity ratios. The derived scaling relations hold promise for integration into pore network models, facilitating the exploration of viscous coupling effect on wetting film and induced dynamic variation of interface instability at pore scale such as main-terminal meniscus and arc-meniscus (Al-Gharbi and Blunt, 2005; Dong and Chatzis, 1995; Li et al., 2017).

### CRedit authorship contribution statement

**Wenbo Gong:** Investigation, Validation, Writing – original draft. **Yang Liu:** Investigation, Software. **Wenhai Lei:** Investigation, Validation. **Yang Ju:** Investigation, Writing – review & editing. **Moran Wang:** Conceptualization, Formal analysis, Methodology, Supervision, Project administration, Writing – review & editing.

### Declaration of Competing Interest

The authors declare that they have no known competing financial interests or personal relationships that could have appeared to influence the work reported in this paper.

### Data availability

No data was used for the research described in the article.

### Acknowledgments

This work is financially supported by the NSF grant of China (no. 12272207) and the National Key Research and Development Program of China (no. 2019YFA0708704).

$$g = \frac{\pi(R^{eff})^4}{8\mu} \tag{A.1}$$

$$R^{eff} = \sqrt{4\pi R}$$

By replacing the radius  $R$  with a cross-section area  $A$ , we could rewrite the above formulation of fluid conductance in a square pore:

$$g = 0.6366 \frac{GA^2}{\mu} \tag{A.2}$$

where the cross-section area in the square capillary  $A = 4R^2$  and its shape factor  $G = \frac{1}{16}$ ,  $\mu$  is the dynamic viscosity.

Similarly, (Patzek and Silin, 2001) fitted the hydraulic conductance in the square capillaries using the finite element method, and the proposed formulation of fluid conductance is:

$$g = 0.5623 \frac{GA^2}{\mu} \tag{A.3}$$

For the immiscible two-phase flow in a capillary tube, the conductance of each fluid was computed separately. The two-phase hydraulic conductance correlation was first used by the Ransohoff-Radke scaling (Ransohoff and Radke, 1988), and then was simplified by (Øren et al., 1998). When the wetting phase is present at the arc-meniscus in a corner with a contact angle  $\theta$  less than  $90^\circ - \beta$  ( $\beta$  is the half angle of the corner in the cross-section), the conductance  $g_k^w$  in corner  $k$  is

$$g_k^w = \frac{(r_c)^2 A_k^w}{C_k^w \mu_w} \tag{A.4}$$

where the radius of curvature of the immiscible interface  $r_c = \gamma/P_c$  set by the prevailing capillary pressure,  $P_c$ , and the interfacial tension  $\gamma$ ;  $A_k^w$  stands for the cross-section area of filament flow, and  $C_k^w$  is the Ransohoff-Radke dimensionless resistance factor that depends on the corner geometry, the contact angle, and the boundary condition at the immiscible interface. The total conductance is the sum of all the corner conductance. The Patzek-Kristensen scaling predicts the wetting phase hydraulic conductance better, in which the fluid conductance is defined as:

$$g_{w0} = 2 \frac{\tilde{g}_w b^4}{\mu_w} \tag{A.5}$$

where  $\tilde{g}_w$  is the dimensionless conductance of wetting fluid, and  $b$  is the meniscus-apex distance along the wall. For a square cross-section, the dimensionless conductance can be computed using a semi-empirical model with a no-slip boundary condition between the wetting and nonwetting fluids:

$$\tilde{g}_w = \exp \left\{ \frac{\left[ -15.1794(\tilde{G}^w)^2 + 7.6307\tilde{G}^w - 0.53488 + 0.02\sin\left(\beta - \frac{\pi}{6}\right) \right]}{(0.25\pi - \tilde{G}^w)\sqrt{\cos\left(\beta - \frac{\pi}{6}\right)\left(\frac{0.25}{\pi} - \tilde{G}^w\right)^{7/8}}} + 2\ln\tilde{A}^w \right\} \tag{A.6}$$

$$\tilde{G}^w = \tilde{A}^w / 4 \left[ 1 - \left(\theta + \beta - \frac{\pi}{2}\right) \sin\beta / \cos(\theta + \beta) \right]$$

$$\tilde{A}^w = \left[ \frac{\sin\beta}{\cos(\theta + \beta)} \right]^2 \left[ \left[ \frac{\cos\theta\cos(\theta + \beta)}{\sin\beta} + \theta + \beta - \frac{\pi}{2} \right] \right]$$

A new scheme for the hydraulic conductance of the wetting fluid occupying the corner was proposed in the work of (Valvatne and Blunt, 2004):

$$g_{w0} = C \frac{b^4 (\tilde{A}^w)^2 \tilde{G}^w}{\mu_w} \tag{A.7}$$

$$C = 0.364 + 0.28 \frac{G^*}{\tilde{G}^w}$$

$$G^* = \frac{\sin\beta\cos\beta}{4(1 + \sin\beta)^2}$$

(Joekar-Niasar et al., 2010) rewrote the conductance formulation in a square cross-section following Ransohoff and Radke:

$$g_k^w = \frac{(r_c)^4 (4 - \pi)}{C_k^w \mu_w} \tag{A.8}$$

Two conditions are required in this conductance equation, including a square cross-section and zero contact angle. A general type of wetting fluid conductance in the square tube with arbitrary contact angles is

$$g_k^w = \frac{(r_c)^4 (4\cos^2\theta - 4\cos\theta\sin\theta - \pi + 4\theta)}{C_k^w \mu_w} \tag{A.9}$$

Previous studies mainly focused on the prediction of the wetting-fluid conductance along the corner of the cross-section, and a few studies discussed the hydraulic conductance of the non-wetting fluid occupying the center space. (Øren et al., 1998) proposed that the conductance of non-wetting fluid occupying the pore center was computed using the scheme of single-phase conductance but with  $A$  replaced by the cross-section area

occupied by the non-wetting phase,  $A_n$ :

$$g_{n0} = 0.5623 \frac{GA_n^2}{\mu_n} \quad (\text{A.10})$$

(Joekear-Niasar et al., 2010) gave a different expression of the nonwetting-fluid conductance:

$$g_{n0} = \frac{\pi}{8\mu_n} (r^{eff})^4$$

$$r^{eff} = \frac{1}{2} \left( \sqrt{\frac{r^2 - (4 - \pi)r_c^2}{\pi}} + r \right) \quad (\text{A.11})$$

where  $r$  is the radius of the pore throat. This formulation used the scheme of circular capillary conductance with an effective radius that is the average of the throat radius and the equivalent radius of the non-wetting-fluid area in the cross-section. Particularly, the formulation is only suitable for the perfectly wetting fluid with zero contact angle.

## Appendix B: Validation of single-phase conductance in a square capillary

The finite differential method (FDM) is used to solve the partial differential equation (Eq. (6)) for single-phase flow, and the discrete scheme is:

$$4u_{ij} - u_{i+1j} - u_{i-1j} - u_{ij+1} - u_{ij-1} = f_{ij}^* dx^2 \quad (\text{B.1})$$

where the global pressure difference is fixed at zero and the space is discretized as plenty of nodes with equal spatial intervals along the x-axis and the y-axis,  $dx$ . A constant body force  $f_{ij}^*$  is applied to drive the fluid flow in a square capillary.

To solve the velocity field in a square capillary tube with infinite length and radius  $R$ , the simulation only calculates a quarter of the square section. As shown in Fig. 1, the zero-velocity boundary condition is used for the solid wall (solid line) in the modeling,  $u_{ij} = 0$ , and the symmetrical boundary condition is used in the fluid boundary (dash line),  $\nabla u \cdot \vec{n} = 0$ . The finite difference scheme of the fluid boundary condition is:

$$(nx + ny)u_{ij} - nx * u_{i-1j} - ny * u_{i-1j} = 0 \quad (\text{B.2})$$

To validate the finite differential scheme, we compute the velocity field of a single phase driven by the body force in the square section. The computational parameters contain the body force  $f = 1\text{N/m}^3$ , fluid viscosity  $\mu = 0.001\text{Pa} \cdot \text{s}$ , and the node number  $Nx = Ny = 1001$ . The total flux in the square section is:

$$Q = \int u dA = \sum u * dx dy \quad (\text{B.3})$$

Thus, the fluid conductance in the square section is defined as:

$$g = \frac{Q}{f} \quad (\text{B.4})$$

Performing a series of FDM simulations in the square section with varying pore sizes, a comparison of the fluid conductance between the predicted formulations and the calculated result in this study indicates that the Patzek-Kristensen scaling approach matches better. The scaling models of the fluid conductance in a square capillary tube are summarized in Appendix A.

## References

- Al-Futaisi, A., Patzek, T.W., 2003. Impact of wettability alteration on two-phase flow characteristics of sandstones: a quasi-static description. *Water Resour. Res.* 39, 1042. <https://doi.org/10.1029/2002wr001366>.
- Al-Gharbi, M.S., Blunt, M.J., 2005. Dynamic network modeling of two-phase drainage in porous media. *Phys. Rev. E Stat. Nonlin. Soft Matter Phys.* 71, 016308 <https://doi.org/10.1103/PhysRevE.71.016308>.
- Andersen, P.Ø., Nesvik, E.K., Standnes, D.C., 2020. Analytical solutions for forced and spontaneous imbibition accounting for viscous coupling. *J. Pet. Sci. Eng.* 186, 106717 <https://doi.org/10.1016/j.petrol.2019.106717>.
- Andersen, P.Ø., Qiao, Y., Standnes, D.C., Evje, S., 2019. Cocurrent spontaneous imbibition in porous media with the dynamics of viscous coupling and capillary backpressure. *SPE J.* 24, 158–177.
- Atyabi, S.A., Afshari, E., 2019. Three-dimensional multiphase model of proton exchange membrane fuel cell with honeycomb flow field at the cathode side. *J. Clean. Prod.* 214, 738–748. <https://doi.org/10.1016/j.jclepro.2018.12.293>.
- Azzam, M., Dullien, F., 1977. Flow in tubes with periodic step changes in diameter a numerical solution. *Chem. Eng. Sci.* 32, 1445–1455.
- Baroutaji, A., Wilberforce, T., Ramadan, M., Olabi, A.G., 2019. Comprehensive investigation on hydrogen and fuel cell technology in the aviation and aerospace sectors. *Renew. Sustain. Energy Rev.* 106, 31–40. <https://doi.org/10.1016/j.rser.2019.02.022>.
- Bentsen, R.G., 1998b. Effect of momentum transfer between fluid phases on effective mobility. *J. Pet. Sci. Eng.* 21, 27–42. [https://doi.org/10.1016/S0920-4105\(98\)00035-7](https://doi.org/10.1016/S0920-4105(98)00035-7).
- Bentsen, R.G., 1998a. Influence of hydrodynamic forces and interfacial momentum transfer on the flow of two immiscible phases. *J. Pet. Sci. Eng.* 19, 177–190. [https://doi.org/10.1016/S0920-4105\(97\)00021-1](https://doi.org/10.1016/S0920-4105(97)00021-1).
- Bourbiaux, B.J., Kalaydjian, F.J., 1990. Experimental Study of Cocurrent and Countercurrent Flows in Natural Porous Media. *SPE Reserv. Eng.* 5, 361–368. <https://doi.org/10.2118/18283-PA>.
- Christou, K., Radünz, W.C., Lashore, B., de Oliveira, F.B.S., Gomes, J.L.M.A., 2019. Numerical investigation of viscous flow instabilities in multiphase heterogeneous porous media. *Adv. Water Res.* 130, 46–65. <https://doi.org/10.1016/j.advwatres.2018.10.010>.
- Dehghanpour, H., Aminzadeh, B., DiCarlo, D.A., 2011. Hydraulic conductance and viscous coupling of three-phase layers in angular capillaries. *Phys. Rev. E* 83, 066320. <https://doi.org/10.1103/PhysRevE.83.066320>.
- Dong, M., Chatzis, I., 1995. The Imbibition and Flow of a Wetting Liquid along the Corners of a Square Capillary Tube. *J. Colloid Interface Sci.* 172, 278–288. <https://doi.org/10.1006/jcis.1995.1253>.
- Ehrlich, R., 1993. Viscous coupling in two-phase flow in porous media and its effect on relative permeabilities. *Transp. Porous Media* 11, 201–218. <https://doi.org/10.1007/BF00614812>.
- Gunstensen, A.K., Rothman, D.H., 1993. Lattice-Boltzmann studies of immiscible two-phase flow through porous media. *J. Geophys. Res.: Solid Earth* 98, 6431–6441. <https://doi.org/10.1029/92JB02660>.
- Guo, B., Zeng, J., Brusseau, M.L., Zhang, Y., 2022. A screening model for quantifying PFAS leaching in the vadose zone and mass discharge to groundwater. *Adv. Water Res.* 160, 104102 <https://doi.org/10.1016/j.advwatres.2021.104102>.
- Hu, R., Wan, J., Kim, Y., Tokunaga, T.K., 2017. Wettability effects on supercritical CO<sub>2</sub>-brine immiscible displacement during drainage: pore-scale observation and 3D

- simulation. *Int. J. Greenhouse Gas Control* 60, 129–139. <https://doi.org/10.1016/j.jggc.2017.03.011>.
- Huang, H., Li, Z., Liu, S., Lu, X-y, 2009. Shan-and-Chen-type multiphase lattice Boltzmann study of viscous coupling effects for two-phase flow in porous media. *Int. J. Numer. Methods Fluids* 61, 341–354. <https://doi.org/10.1002/fld.1972>.
- Huang, H., Lu, X-y, 2009. Relative permeabilities and coupling effects in steady-state gas-liquid flow in porous media: a lattice Boltzmann study. *Phys. Fluid.* 21, 092104 <https://doi.org/10.1063/1.3225144>.
- Jiang, F., Yang, J., Boek, E., Tsuji, T., 2021. Investigation of viscous coupling effects in three-phase flow by lattice Boltzmann direct simulation and machine learning technique. *Adv. Water Res.* 147, 103797 <https://doi.org/10.1016/j.advwatres.2020.103797>.
- Joekar-Niasar, V., Hassanizadeh, S.M., Dahle, H.K., 2010. Non-equilibrium effects in capillarity and interfacial area in two-phase flow: dynamic pore-network modelling. *J. Fluid Mech.* 655, 38–71. <https://doi.org/10.1017/s0022112010000704>.
- Ju, Y., Gong, W., Chang, W., Sun, M., 2020. Effects of pore characteristics on water-oil two-phase displacement in non-homogeneous pore structures: a pore-scale lattice Boltzmann model considering various fluid density ratios. *Int. J. Eng. Sci.* 154, 103343 <https://doi.org/10.1016/j.jengsci.2020.103343>.
- Kalaydjian, F., 1990. Origin and quantification of coupling between relative permeabilities for two-phase flows in porous media. *Transp. Porous Media* 5, 215–229. <https://doi.org/10.1007/BF00140013>.
- Legait, B., 1983. Laminar flow of two phases through a capillary tube with variable square cross-section. *J. Colloid Interface Sci.* 96, 28–38. [https://doi.org/10.1016/0021-9797\(83\)90005-X](https://doi.org/10.1016/0021-9797(83)90005-X).
- Lei, W., Lu, X., Liu, F., Wang, M., 2022. Non-monotonic wettability effects on displacement in heterogeneous porous media. *J. Fluid Mech.* 942, R5. <https://doi.org/10.1017/jfm.2022.386>.
- Lei, W., Lu, X., Wang, M., 2023. Multiphase displacement manipulated by micro/nanoparticle suspensions in porous media via microfluidic experiments: from interface science to multiphase flow patterns. *Adv. Colloid Interface Sci.* 311, 102826 <https://doi.org/10.1016/j.cis.2022.102826>.
- Lenormand, R., Touboul, E., Zarcone, C., 1988. Numerical models and experiments on immiscible displacements in porous media. *J. Fluid Mech.* 189, 165–187. <https://doi.org/10.1017/S0022112088000953>.
- Li, H., Pan, C., Miller, C.T., 2005. Pore-scale investigation of viscous coupling effects for two-phase flow in porous media. *Phys. Rev. E* 72, 026705. <https://doi.org/10.1103/PhysRevE.72.026705>.
- Li, J., McDougall, S.R., Sorbie, K.S., 2017. Dynamic pore-scale network model (PNM) of water imbibition in porous media. *Adv. Water Res.* 107, 191–211. <https://doi.org/10.1016/j.advwatres.2017.06.017>.
- Liu, F., Wang, M., 2020. Review of low salinity waterflooding mechanisms: wettability alteration and its impact on oil recovery. *Fuel* 267, 117112. <https://doi.org/10.1016/j.fuel.2020.117112>.
- Liu, F., Wang, M., 2022b. Wettability effects on mobilization of ganglia during displacement. *Int. J. Mech. Sci.* 215, 106933 <https://doi.org/10.1016/j.ijmecsci.2021.106933>.
- Liu, T., Wang, M., 2022a. Critical REV Size of Multiphase Flow in Porous Media for Upscaling by Pore-Scale Modeling. *Transp. Porous Media* 144, 111–132. <https://doi.org/10.1007/s11242-021-01621-2>.
- Øren, P.E., Bakke, S., Arntzen, O.J., 1998. Extending predictive capabilities to network models. *SPE J.* 3, 324–336.
- Patzek, T.W., Kristensen, J.G., 2001. Shape factor correlations of hydraulic conductance in noncircular capillaries. *J. Colloid Interface Sci.* 236, 305–317. <https://doi.org/10.1006/jcis.2000.7414>.
- Patzek, T.W., Silin, D.B., 2001. Shape factor and hydraulic conductance in noncircular capillaries. *J. Colloid Interface Sci.* 236, 295–304. <https://doi.org/10.1006/jcis.2000.7413>.
- Primkulov, B.K., Pahlavan, A.A., Fu, X., Zhao, B., MacMinn, C.W., Juanes, R., 2019. Signatures of fluid–fluid displacement in porous media: wettability, patterns and pressures. *J. Fluid Mech.* 875, R4. <https://doi.org/10.1017/jfm.2019.554>.
- Primkulov, B.K., Pahlavan, A.A., Fu, X., Zhao, B., MacMinn, C.W., Juanes, R., 2021. Wettability and Lenormand's diagram. *J. Fluid Mech.* 923, A34. <https://doi.org/10.1017/jfm.2021.579>.
- Qiao, Y., Andersen, P.Ø., Evje, S., Standnes, D.C., 2018. A mixture theory approach to model co- and counter-current two-phase flow in porous media accounting for viscous coupling. *Adv. Water Res.* 112, 170–188. <https://doi.org/10.1016/j.advwatres.2017.12.016>.
- Qin, C.-Z., van Brummelen, H., 2019. A dynamic pore-network model for spontaneous imbibition in porous media. *Adv. Water Res.* 133, 103420 <https://doi.org/10.1016/j.advwatres.2019.103420>.
- Rabbani, H.S., Joekar-Niasar, V., Pak, T., Shokri, N., 2017. New insights on the complex dynamics of two-phase flow in porous media under intermediate-wet conditions. *Sci. Rep.* 7, 4584. <https://doi.org/10.1038/s41598-017-04545-4>.
- Rakotomalala, N., Salin, D., Yortsos, Y.C., 1995. Viscous coupling in a model porous medium geometry: effect of fluid contact area. *Appl. Sci. Res.* 55, 155–169. <https://doi.org/10.1007/BF00868469>.
- Ramakrishnan, T.S., Goode, P.A., 2015. Measurement of off-diagonal transport coefficients in two-phase flow in porous media. *J. Colloid Interface Sci.* 449, 392–398. <https://doi.org/10.1016/j.jcis.2015.01.029>.
- Ramstad, T., Øren, P.-E., Bakke, S., 2010. Simulation of two-phase flow in reservoir rocks using a lattice Boltzmann method. *SPE J.* 15, 917–927. <https://doi.org/10.2118/124617-PA>.
- Ransohoff, T.C., Radke, C.J., 1988. Laminar flow of a wetting liquid along the corners of a predominantly gas-occupied noncircular pore. *J. Colloid Interface Sci.* 121, 392–401.
- Roman, S., Soullaine, C., Kovscek, A.R., 2020. Pore-scale visualization and characterization of viscous dissipation in porous media. *J. Colloid Interface Sci.* 558, 269–279. <https://doi.org/10.1016/j.jcis.2019.09.072>.
- Rose, W., 1997. An upgraded viscous coupling measurement methodology. *Transp. Porous Media* 28, 221–231. <https://doi.org/10.1023/A:1006596830724>.
- Sethian, J.A., Smereka, P., 2003. Level set methods for fluid interfaces. *Annu. Rev. Fluid Mech.* 35, 341–372. <https://doi.org/10.1146/annurev.fluid.35.101101.161105>.
- Shams, M., Raeini, A.Q., Blunt, M.J., Bijeljic, B., 2018. A study to investigate viscous coupling effects on the hydraulic conductance of fluid layers in two-phase flow at the pore level. *J. Colloid Interface Sci.* 522, 299–310. <https://doi.org/10.1016/j.jcis.2018.03.028>.
- Singhal, A.K., Somerton, W.H., 1970. Two-phase flow through a non-circular capillary at low Reynolds numbers. *J. Can. Pet. Technol.* 9, PETSOC-70-03-5.
- Solazzi, S.G., Jougnot, D., Rubino, J.G., Holliger, K., 2023. Dynamic relative permeabilities for partially saturated porous media accounting for viscous coupling effects: an analytical solution. *Transp. Porous Media* 147, 653–677. <https://doi.org/10.1007/s11242-023-01920-w>.
- Spirin, C., Bultreys, T., Rucker, M., Garfi, G., Schlepütz, C.M., Novak, V., et al., 2021. The development of intermittent multiphase fluid flow pathways through a porous rock. *Adv. Water Res.* 150, 103868 <https://doi.org/10.1016/j.advwatres.2021.103868>.
- Valvatne, P.H., Blunt, M.J., 2004. Predictive pore-scale modeling of two-phase flow in mixed wet media. *Water Resour. Res.* 40. <https://doi.org/10.1029/2003wr002627>.
- Xie, C., Raeini, A.Q., Wang, Y., Blunt, M.J., Wang, M., 2017. An improved pore-network model including viscous coupling effects using direct simulation by the lattice Boltzmann method. *Adv. Water Res.* 100, 26–34. <https://doi.org/10.1016/j.advwatres.2016.11.017>.
- Yazzan, S.K., Bentsen, R.G., Trivedi, J., 2013. Sensitivity analysis for dynamic spontaneous imbibition with variable inlet saturation and interfacial coupling effects. *Transp. Porous Media* 96, 397–417. <https://doi.org/10.1007/s11242-012-0095-9>.
- Yiotis, A.G., Pshogios, J., Kainourgiakis, M.E., Papaioannou, A., Stubos, A.K., 2007. A lattice Boltzmann study of viscous coupling effects in immiscible two-phase flow in porous media. *Colloids Surf. A* 300, 35–49. <https://doi.org/10.1016/j.colsurfa.2006.12.045>.
- Yuster, S.T., 1951. Theoretical considerations of multiphase flow in idealized capillary systems. In: *The 3rd World Petroleum Congress*. The Hague, the Netherlands.
- Zarcone, C., Lenormand, R., 1994. Détermination expérimentale du couplage visqueux dans les écoulements diphasiques en milieu poreux. *CR Acad. Sci. Paris Ser. II* 318, 1429–1438.
- Zhao, J., Qin, F., Kang, Q., Qin, C., Derome, D., Carmeliet, J., 2022. A dynamic pore network model for imbibition simulation considering corner film flow. *Water Resour. Res.* 58, e2022WR032332 <https://doi.org/10.1029/2022WR032332>.